# Cylindrical Surface Wave on Periodically Corrugated Metal*)

Kazuo OGURA, Hiroshi IIDUKA and Kiyoyuki YAMBE

*Graduate School of Science and Technology, Niigata University, Niigata 950-2181, Japan*

(Received 9 December 2011 / Accepted 12 February 2012)

We present a numerical and experimental study of the dispersion characteristics of cylindrical surface waves on metallic cylinders with rectangular corrugations. In actual devices, reflections at both ends quantize the electromagnetic modes into resonant axial modes. A cavity method based on axial mode measurements is applied to study the properties of the cylindrical surface waves. The resonances are relatively sharp near the upper cutoff, but at low frequencies far from the cutoff, the resonances broaden to resemble those of a Sommerfeld wave.



Keywords: cylindrical surface wave, periodical corrugation, axial mode, surface plasmon, Sommerfeld wave

DOI: 10.1585/pfr.7.2406022

## 1. Introduction

Smith–Purcell free-electron lasers (SP-FELs) [1] have been studied as conceivable electromagnetic wave sources covering the microwave–terahertz range. In SP-FELs, an electron beam passes by a periodic corrugation and excites spatial harmonics called Floquet harmonics. The SP radiation occurs spontaneously when the excited harmonics are in the fast-wave region. In addition to fast waves, the periodic corrugation supports slow waves that do not radiate directly. The slow wave provides a feedback to form a beam bunch via a backward-wave operation, which leads to stimulated radiations called super radiance [2, 3]. Stimulated SP radiation was first demonstrated by using the beam from a scanning electron microscope (SEM) in Ref. [2] and this technique has attracted attention as a way to develop a compact terahertz wave source.

The SP devices mentioned above are commonly based on a plane geometry. Another realistic geometry is cylindrical, which is very effective for high-power backward-wave oscillators (BWOs). The concept of stimulated SP radiations incorporating cylindrical BWOs appears very attractive for improving the radiation intensity. A backward-wave oscillation was examined on the basis of a cylindrical surface wave (CSW) [4] and a preliminary experiment demonstrated the generation of SP radiations on the basis of CSWs in a frequency range about four times higher than the CSW frequency [5]. In actual devices, CSWs are reflected at the corrugated ends and form standing waves along the axial direction. To understand the generation of stimulated SP radiation via backward-wave operation, CSWs and axial modes need to be further studied.

We present herein a numerical and experimental study of CSWs. In our experiments, we apply a cavity method based on axial mode measurements and developed for BWOs [6] to study the properties of CSWs. On corrugated metal surfaces, Sommerfeld waves [7], which originate from surface plasmons, coexist with CSWs and now attract a renewed attention for terahertz wave guiding [8]. We examine the axial mode properties of CSWs by comparing them with the properties of Sommerfeld waves.

## 2. Formulation of Cylindrical Surface Waves

We consider a corrugated metallic cylinder inside a hollow pipe, as shown in Fig. 1. The parameters are the average corrugation radius $R_0$, the corrugation amplitude $h$, the corrugation width $d$, the periodic corrugation length $z_0$, and the radius $R_1$ of the hollow pipe. The corrugation wave number is given by $k_0 = 2\pi/z_0$. A mathematical formulation for a hollow waveguide with a rectangular corrugation is presented in Ref. [9] and we apply this formulation to the configuration shown in Fig. 1.

In rectangular corrugation (region I; $R_0 - h < r < R_0 + h$), the electromagnetic waves may be expressed by a sum of standing waves that satisfy the boundary conditions at the wall of the rectangular corrugation. In the region between the inner cylinder and the wall of the hollow pipe (region II; $R_0 + h < r < R_1$), the electromagnetic field is expanded in a spatial harmonic series according to Floquet theorem:

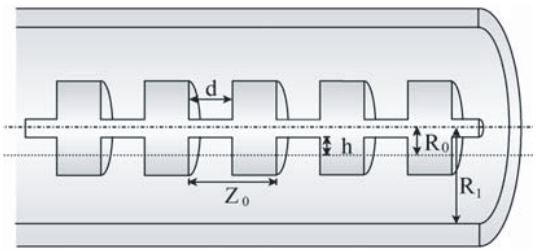


Fig. 1 Schematic of a corrugated cylinder inside a hollow pipe.

*author's e-mail: teogura@eng.niigata-u.ac.jp*

*) This article is based on the presentation at the 21st International Toki Conference (ITC21).

$$E_z^{\mathrm{II}} = \sum_{p=-\infty}^{\infty} \left[ D_p J_m(x_p r) + E_p N_m(x_p r) \right],$$
$$B_z^{\mathrm{II}} = \sum_{p=-\infty}^{\infty} \frac{\mathrm{i}}{c} \left[ F_p J_m(x_p r) + G_p N_m(x_p r) \right]. \quad (1)$$

Here, $J_m$ and $N_m$ denote the $m$th-order Bessel function of the first kind and of the second kind, respectively, where $m$ is the azimuthal mode number. The wave number $k_p$ satisfies the relation $k_p = k_z + pk_0$, where $p$ is Floquet harmonic number, $k_z$ is the axial wave number, and

$$x_p^2 = \frac{\omega^2}{c^2} - k_p^2, \quad (2)$$

with $\omega$ being the angular frequency. The constants $D_p$, $E_p$, $F_p$, and $G_p$ are the coefficients of the electromagnetic fields. The other field components can be derived from $E_z$ and $B_z$. When the waves become slow with a phase velocity less than the speed of light, the Bessel functions are replaced by the modified Bessel functions of the first kind $I_m$ and of the second kind $K_m$.

The normal modes of the system are derived subject to the boundary conditions. The fields in the regions I and II of Fig. 1 must be connected at the boundary. This field-matching condition uniquely relates the standing waves in region I to Floquet harmonics in region II. Thus, the electromagnetic fields in all regions are expressed in terms of $D_p$, $E_p$, $F_p$, and $G_p$. The boundary conditions on the inner corrugation and the outer pipe surface may be expressed, respectively, by the following matrix forms:

$$\begin{bmatrix} \mathrm{D}^{(11)}\mathrm{D}^{(12)}\mathrm{D}^{(13)}\mathrm{D}^{(14)} \\ \mathrm{D}^{(21)}\mathrm{D}^{(22)}\mathrm{D}^{(23)}\mathrm{D}^{(24)} \end{bmatrix} \cdot \begin{bmatrix} \mathbf{D} \\ \mathbf{E} \\ \mathbf{F} \\ \mathbf{G} \end{bmatrix} = 0, \quad (3)$$

$$\begin{bmatrix} \mathrm{D}^{(31)}\mathrm{D}^{(32)}\mathrm{D}^{(33)}\mathrm{D}^{(34)} \\ \mathrm{D}^{(41)}\mathrm{D}^{(42)}\mathrm{D}^{(43)}\mathrm{D}^{(44)} \end{bmatrix} \cdot \begin{bmatrix} \mathbf{D} \\ \mathbf{E} \\ \mathbf{F} \\ \mathbf{G} \end{bmatrix} = 0. \quad (4)$$

Here, **D**, **E**, **F**, and **G** denote column vectors with elements $D_p$, $E_p$, $F_p$, and $G_p$, and $\mathrm{D}^{(\mathrm{ij})}$ with $1 \le i, j \le 4$ denote a matrix of infinite rank.

If the hollow pipe in Fig. 1 is removed, the boundary condition at $r = R_1$ is substituted by a condition that the electromagnetic fields approach zero as $r$ tends to $\infty$. In this case, $\mathbf{D} = 0$ and $\mathbf{F} = 0$, and the boundary conditions on the cylindrical corrugation becomes

$$\begin{bmatrix} \mathrm{D}^{(12)}\mathrm{D}^{(14)} \\ \mathrm{D}^{(22)}\mathrm{D}^{(24)} \end{bmatrix} \cdot \begin{bmatrix} \mathbf{E} \\ \mathbf{G} \end{bmatrix} = 0. \quad (5)$$

## 3. Dispersion Characteristics

The dispersion characteristics are given by the condition that Eqs. (3) and (4) have nontrivial solutions, which leads to

$$\det \begin{bmatrix} \mathrm{D}^{(11)}\mathrm{D}^{(12)}\mathrm{D}^{(13)}\mathrm{D}^{(14)} \\ \mathrm{D}^{(21)}\mathrm{D}^{(22)}\mathrm{D}^{(23)}\mathrm{D}^{(24)} \\ \mathrm{D}^{(31)}\mathrm{D}^{(32)}\mathrm{D}^{(33)}\mathrm{D}^{(34)} \\ \mathrm{D}^{(41)}\mathrm{D}^{(42)}\mathrm{D}^{(43)}\mathrm{D}^{(44)} \end{bmatrix} = 0. \quad (6)$$

Similarly, the dispersion characteristics for $R_1$ infinite is obtained from Eq. (5) as,

$$\det \begin{bmatrix} \mathrm{D}^{(12)}\mathrm{D}^{(14)} \\ \mathrm{D}^{(22)}\mathrm{D}^{(24)} \end{bmatrix} = 0. \quad (7)$$

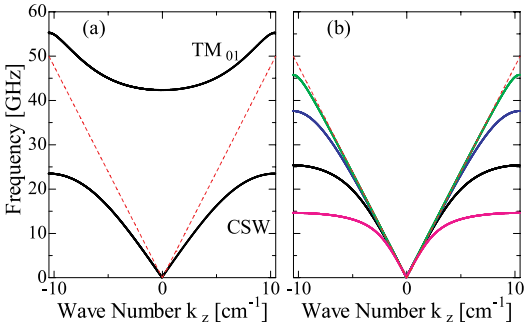


Fig. 2 Dispersion curves of corrugated cylinder (a) with and (b) without hollow pipe. Dotted lines represent light lines. In (b), starting with the upper-most solid curve, $h$ takes the values 0.25, 0.5, 1.0 and 2.0 mm.

The dispersion curves for Fig. 1 are plotted in Fig. 2 (a) with $R_0 = 13$ mm, $d = 1.5$ mm, $z_0 = 3.0$ mm, $h = 1.0$ mm, and $R_1 = 15$ mm. According to Floquet theorem, the dispersion curves are periodic in wave number space ($k_z$-space) with a period $k_0 = 20.9\,\mathrm{cm}^{-1}$. In Fig. 2 (a), the reduced-zone scheme is shown for a period from $-k_0/2$ to $k_0/2$. The meaning of the backward wave based on this scheme is equivalent to that of BWO in Refs. [3, 4], where the dispersion curves are plotted for $0 < k_z < 2\pi/z_0$ on the basis of the periodic-zone scheme. Generally, a coaxial cylinder in a hollow pipe generates a transverse electromagnetic (TEM) mode: a mode without a lower cutoff frequency. When the inner cylinder is corrugated, as shown in Fig. 1, the TEM mode transforms into a CSW, which is a slow wave with an upper cutoff frequency at the $\pi$ point ($k_z z_0 = \pi$). Furthermore, the CSW has a finite $E_z$ originating from the corrugation.

The transverse magnetic (TM) mode in Fig. 2 (a) is a fast wave because of the pipe whose lower cutoff can be below the upper cutoff of the CSW. In this case, the TM mode and the CSW may overlap. The lower cutoff of the TM mode is shifted up by decreasing the distance between the inner and the outer cylinders. For the dimensions given in Fig. 2 (a), the TM mode exists well above the CSW cutoff leading to a stop band.

The CSW can exist even if the outer pipe is removed. In this case, the dispersion characteristics are given by Eq. (7) and potted in Fig. 2 (b) with $R_0 = 13.0$ mm, $d =$

1.5 mm, and $z = 3.0$ mm and for various values of $h$. Upon increasing $h$, the upper cutoff frequency at the $\pi$ point decreases. As we approach the $\pi$ point, the CSW departs from the light line because of a reduction in its phase velocity. Near the $\pi$ point, the CSW has a relatively short attenuation length and is localized very close to the corrugation surface.

## 4. Axial Modes of Cylindrical Surface Waves

For finite-length corrugations, the boundary conditions at both ends ($z = 0$ and $z = L$) are imposed, in addition to Eq. (6) or (7). A forward-propagating wave reflects at $z = L$ and transforms into a backward-propagating wave, which leads to axial modes. Except for the propagation direction, the backward wave is identical to the forward wave. For simplicity, we show only $k_z$ for the forward wave like Fig. 3 (c), where the axial modes are equally spaced, and $k_z$ takes on the values of $\pi N/L$, where $N$ is a natural number

First, we elucidate the axial mode excitation within a waveguide cavity, as shown in Fig. 3. For the closed cavity, a small wire antenna can be employed to excite axial modes. A network analyzer is used to measure the scattering parameters: the microwave reflection from the structure ($S_{11}$) and the transmission through the structure ($S_{21}$). The resonances appear as spikes where $S_{11}$ decreases while $S_{21}$ increases. The measured results are shown in Figs. 3 (b) and (c). The clear peaks in $S_{11}$ and $S_{21}$ correspond to axial modes with $k_z = \pi N/L$.

We inserted the corrugated cylinder on the axis of Fig. 3 (a) and measured the axial modes for the parameters of Fig. 2 (a). The results are given in Fig. 4. The stop band corresponding to Fig. 2 (a) is evident. The length of the corrugated cylinder is $L = 10z_0$, so the wave number $N/L$ of the axial mode can be changed from $N = 0$ to 10. The axial mode at $k_z z_0 = 9\pi/10$ can be identified, but the axial mode at the $\pi$ point ($N = 10$) is not observed (Fig. 4). In addition, the other peaks of $S_{11}$ and $S_{21}$ are not identified as axial modes of the CSW, which may be due to a poor coupling of the antenna to the CSW and additional resonant modes caused by the excitation section composed of the antenna and pipe. The measurement of the CSW is very complicated, even though the CSW and TM modes exist independently.

To avoid the effects of the surrounding pipe, we have removed it, as indicated in Fig. 5 (a). In this case, the coupling of the wire antenna to the CSW weakens, so we added a disk to the wire tip. After cautiously adjusting parallelism between the disk, flange, and corrugation, the

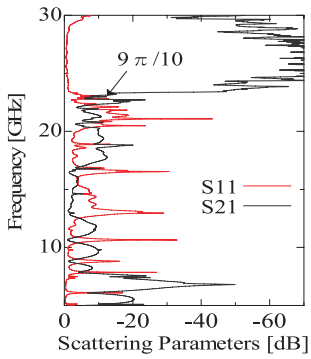


Fig. 4 Profiles of $S_{11}$ and $S_{21}$ for the corrugation of Fig. 2 (a) with $L = 10z_0$.

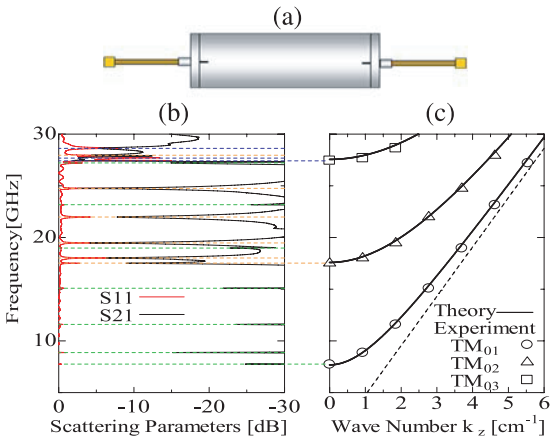


Fig. 3 (a) Schematic of cylindrical cavity. (b) $S_{11}$ and $S_{21}$ profiles, and (c) frequency versus wave number for a cylinder of 15 mm radius and 34 mm length. In (b), the green, red and blue dotted lines correspond to $TM_{01}$, $TM_{02}$ and $TM_{03}$ axial modes, respectively, which are shown in (c). The dashed line in (c) is the light line.

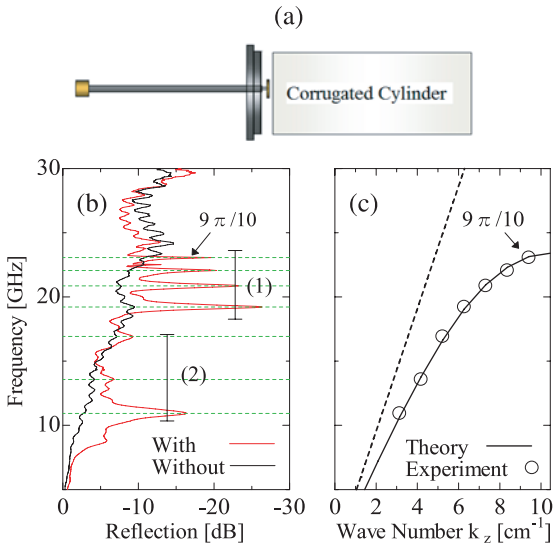


Fig. 5 (a) Schematic of corrugated cylinder (b) $S_{11}$ profiles of axial mode, and (c) frequency versus wave number for CSW. The parameters are the same as those of Fig. 2 (b) with $h = 1.0$ mm. Green dotted lines in (b) correspond to the CSW axial mode in (c). The dashed line in (c) represents the light line.

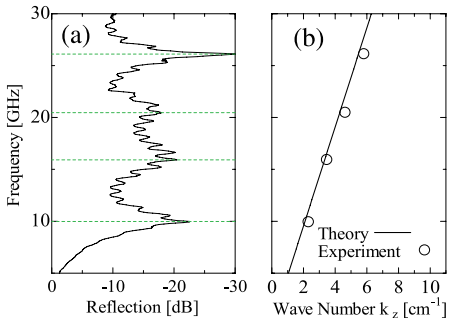


Fig. 6 (a) $S_{11}$ profile of the axial mode and (b) frequency versus wave number for the Sommerfeld wave. Green dotted lines in (b) correspond to axial modes of the Sommerfeld wave in (c).

reflection $S_{11}$ with and without the corrugated cylinder was measured, with the results shown in Fig. 5 (b). The axial modes agree with theoretical values up to $k_z z_0 = 9\pi/10$, as shown in Fig. 5 (c). The $N = 10$ axial mode is not observed. The CSW in the region denoted (1) has $k_z z_0 > 5\pi/10$ and generates sharper resonances than in region (2), where $k_z z_0 \leq 5\pi/10$. The small ripples are attributed to standing waves between the connector and the antenna tip.

We examine the axial modes based on the Sommerfeld wave by replacing the corrugated cylinder with 30-mm-long straight cylinder with a 14 mm radius, which is approximately equal to the dimensions of the corrugated cylinder. The $S_{11}$ resonance peaks, as shown in Fig. 6 (a), correspond to the theoretically expected axial modes due to the Sommerfeld wave, which has almost the same dispersion as the light line in our experiments [10]. The axial modes are broad, similar to the lower-frequency region (2) in Fig. 5 (b). In addition, similar small ripples are observed, as in Fig. 5 (b).

## 5. Discussions and Conclusion

The CSW in region (1) of Fig. 5 (b) possesses a phase velocity that is substantially less than the speed of light and has a small group velocity. The effective impedance is moderately different from that of light waves. Thus, at the corrugated ends, the reflections are comparatively large and the CSW has relatively sharp resonant axial modes, than in region (2) of Fig. 5 (b). To date, the $\pi$ point axial mode has not been observed with or without the surrounding pipe possibly because of a strong reflection of the CSW at the corrugated ends due to a zero group velocity, which would reduce the coupling of the CSW to the antenna.

The CSW will be advantageous in practical applications not only for cylindrical SP-FELs but also for wave guiding, since the properties of the surface waves can be controlled by corrugations [11,12]. By measuring the axial mode, we find that the CSW exhibits two distinctive properties: First, it consists of sharp axial modes in region (1) of Fig. 5 (b), and second, it leads to broadened axial modes in region (2) of Fig. 5 (b). In region (1), the wave length is approximately equal to $z_0$ and the CSWs are well confined to the corrugation surfaces. In region (2), the CSW approaches light and the structural periodicity may be insignificant. Furthermore, the corrugations can be described by the effective surface impedance or the effective dielectric constant. The field properties of the CSW resemble those of a Sommerfeld wave and correspond to the hybrid surface plasmon of Ref. [11].

In conclusion, we have numerically and experimentally analyzed the dispersion characteristics of CSWs on metal cylinders with rectangular corrugations. We have elucidated that the cavity method for a BWO can be applied to study CSWs. The axial modes of CSWs contain relatively sharp resonances near the upper cutoff, showing the well-confined fields. In the region away from the upper cutoff, the axial resonances broaden and become similar to those of a Sommerfeld wave.

[1] S.J. Smith and E.M. Purcell, Phys. Rev. **92**, 1069 (1953).
[2] J. Urata *et al.*, Phys. Rev. Lett. **80**, 516 (1998).
[3] H.L. Andrews *et al.*, Phys. Rev. ST Accel. Beams **12**, 080703 (2009).
[4] K. Ogura *et al.*, Plasma Fusion Res. **6**, 2401039 (2011).
[5] K. Ogura *et al.*, "Preliminary Experiment on Smith-Purcell Radiation Based on Cylindrical Surface Wave", PLASMA2011, 23P146-P (November, 2011, Kanazawa, Japan).
[6] W. Main *et al.*, IEEE Trans. Plasma Sci. **22**, 566 (1994).
[7] H.M. Barlow *et al.*, Radio Section **22**, 329 (1953).
[8] K. Wang *et al.*, Nature **432**, 376 (2004).
[9] Y. Takashima *et al.*, J. Plasma Fusion Res. SERIES **6**, 1512 (2009).
[10] K. Wang and D.M. Mittleman, Phy. Rev. Lett. **96**, 157401 (2006).
[11] J.B. Pendry *et al.*, Science **305**, 847 (2004).
[12] B. Stein *et al.*, Phys. Rev. Lett. **105**, 266804 (2010).